Supporting information

Dipole-aligned polymer electrolyte enabling directed Li^+ migration for all-solid-state Li–S batteries

Wenkai Song, [a] Borui Li, [a] Ran Sun, [a] Keju Chen, [a] Fangyuan Hu*[a] and Xigao Jian [b]

[a] School of Materials Science and Engineering, State Key Laboratory of Fine Chemicals, Frontiers Science Center for Smart Materials Oriented Chemical Engineering, Technology Innovation Center of High Performance Resin Materials (Liaoning Province), Dalian University of Technology, Dalian 116024, China.

[b] State Key Laboratory of Fine Chemicals, Frontiers Science Center for Smart Materials Oriented Chemical Engineering, School of Chemical Engineering, Technology Innovation Center of High Performance Resin Materials (Liaoning Province), Dalian University of Technology, Dalian 116024, China.

*Corresponding author. Email: hufangyuan@dlut.edu.cn (Fangyuan Hu)

Experimental section

1. Materials:

1-ethyl-3-(3-dimethylaminopropyl) carbodiimide hydrochloride (EDC·HCl), 1-hydroxybenzotriazole (HOBt), N, N-diisopropylethylamine (DIPEA), methyl L-alaninate hydrochloride, $NaHCO_3$ and Na_2SO_4 were purchased from Shanghai Macklin Biochemical Co., Ltd. LiFSI, Super P and polyvinylidene difluoride (PVDF) materials were purchased from Canrd.

2. Synthesis Pathways for Polymerizable Monomers:

To a dry 250 mL round-bottom flask equipped with a magnetic stir bar were added 2-ethynylbenzoic acid (1.700 g, 1.2 equiv), 1-ethyl-3-(3-dimethylaminopropyl) carbodiimide hydrochloride (EDC·HCl) (1.350 g, 1.2 equiv), and 1-hydroxybenzotriazole (HOBt) (1.400 g, 1.2 equiv), followed by addition of 70 mL anhydrous CH_2Cl_2. The suspension was cooled slightly and stirred for approx. 15 min to allow in-situ activation of the carboxylic acid, during which the formation of the O-acyl-HOBt intermediate was indicated by the mixture turning clear. Subsequently, N, N-diisopropylethylamine (DIPEA, 1 mL, 2.0 equiv) was added dropwise under continuous stirring to neutralize the acidic by-products and facilitate coupling. After complete mixing, methyl L-alaninate hydrochloride (1.151 g, 1.0 equiv) was introduced in one portion. The reaction mixture was then allowed to stir overnight (~12 h) at room temperature, during which gradual consumption of the starting acid was monitored by TLC. Upon completion, the reaction mixture was transferred to a separatory funnel and washed successively with 1 M HCl (to remove excess amine), saturated $NaHCO_3$ solution (to neutralize acidic residues and unreacted HOBt), and finally brine. The combined organic layers were dried over anhydrous Na_2SO_4, filtered, and concentrated under reduced pressure to yield a pale solid residue. The crude product was purified via silica gel column chromatography (70–230 mesh) using hexane/ethyl acetate (7:3) as the eluent. After collecting and

evaporating the desired fractions, 2.112 g of monomer was obtained as a pure product (80% yield).

3. General Procedure for the Rhodium-Catalyzed Polymerization:

The reaction flask (sealed ampoule) was dried under vacuum and argon flushed for three times before monomer was added as a solid. Then, the flask was evacuated on a vacuum line and flushed with dry argon (three times). Dry THF was added with a syringe and the triethylamine dropwise. A solution of rhodium norbornadiene chloride dimer, $[Rh(nbd)Cl]_2$, in THF was added at 30°C. The reaction mixture was stirring at 30°C for 6 h. Then, the resulting polymer was diluted in CH_2Cl_2 and it was precipitated in a large amount of methanol, centrifuged (2 times), reprecipitated in hexane and centrifuged again.

4. Preparation of Polymer Solid Electrolyte (MPPE):

The dipole-aligned polymer and PVDF-HFP were first dried overnight under vacuum at 60°C to remove residual moisture and solvents. Subsequently, 1.5 g of PVDF-HFP was mixed with different proportion of dipole-aligned polymer in an argon-filled glove box and dissolved in 15 mL of dried DME solvent. The mixture was stirred at 800 rpm for 6 hours at 80°C to form a homogeneous, transparent solution. In a typical preparation, 2.0 g of LiFSI was added to the solution and stirred for at least 2 hours. The stirring speed was then reduced to 200 rpm for 1 hour to ensure uniform dispersion and eliminate microbubbles. The resulting viscous solution was filtered and cast onto a clean PTFE mold. The solvent is slowly evaporated at room temperature, followed by drying the membrane under vacuum at 60°C for 12 hours to remove residual solvent. After cooling to room temperature, the MPPE electrolyte film is carefully peeled off, punched into 16 mm diameter discs, and stored in an argon-filled glove box prior to electrochemical measurements.

5. Preparation of SPAN Cathodes:

The sulfurized polyacrylonitrile (SPAN) was prepared by mixing sulfur (Alfa

Aesar) and polyacrylonitrile (M_w = 150,000, Aldrich) in a weight ratio of 4:1, followed by thermal treatment in an Ar-filled furnace at 450°C for 6 h.

Weigh 0.60 g SPAN, 0.15 g Super P conductive agent, and 0.20 g PVDF-HFP binder by mass ratio. Perform all weighing operations within an argon-filled glove box. Add 3 mL of DME and stir at 800 rpm using a magnetic stirrer at 80°C to form a homogeneous slurry. Subsequently, add 0.25 g of LiFSI and continue stirring for 6 hours until a uniform, fine paste free of visible agglomerates is obtained. The resulting paste is uniformly coated onto carbon-coated aluminum foil using a 250 μm squeegee. After allowing the solvent to evaporate at room temperature, the coated foil is transferred to a vacuum oven and dried overnight at 60°C to ensure complete removal of residual solvent. The dried electrode film was punched into discs of the desired size and sealed for storage in a glove box, ready for subsequent battery assembly experiments.

6. Assembly of Stainless Steel Symmetric batteries:

Assemble the stainless steel symmetric cell within an argon glove box. Use stainless steel discs cut to a diameter of 16 mm as electrodes, thoroughly cleaned and dried beforehand. Cut prepared all-solid-state polymer electrolyte membranes into circular discs matching the electrode size (e.g., 16 mm) and record their thickness (measured using a micrometer with 1 μm precision). During assembly, stack the components in the CR2032 button cell housing in the sequence SS│electrolyte│SS, ensuring the membrane adheres fully to the metal electrodes without wrinkles. Subsequently, insert the spring and gasket. After closing the mold, seal and secure the button cell housing using a press. All symmetric cells are left to rest for 2–4 hours to ensure adequate interface contact before testing.

The ionic conductivity (σ) was calculated by testing the EIS of the blocking batteries over the frequency range of 10^{-1} to 10^{6} Hz using the following formula:

$$\sigma = \frac{L}{SR}$$

where L is the distance between stainless steels; S is the area of the

stainless steel; and R is the impedance.1, 2

7. Assembly of Full batteries:

All battery assembly is performed within an argon glove box. First, the prepared SPAN cathode sheet is punched into 12 mm diameter discs with an active material mass of 1–1.5 mg cm^{-2}. Lithium metal foil serves as the anode, with the all-solid-state polymer electrolyte membrane (MPPE or MPPE@PVDF-HFP) cut into 16 mm diameter discs. Subsequently, assembly is performed within a CR2032 button cell casing in the order: negative electrode | solid electrolyte | positive electrode. Care is taken to ensure the membrane surface is flat and all layers are fully aligned. If necessary, light pressure may be applied to enhance interfacial contact, but excessive compression of the electrolyte membrane must be avoided. After assembly, spacers and spring clips are inserted, and the cell casing is sealed using a hydraulic encapsulation machine. The encapsulated complete cell is then left to rest in a glove box for at least 4–6 hours before proceeding with subsequent electrochemical testing.

8. Electrochemical measurements:

The transference numbers were measured using the Bruce–Vincent–Evans method in Li‖Li symmetric cells. A small DC polarization voltage (ΔV = 10 mV) was applied at room temperature, and the initial (I_0) and steady-state (I_s) currents were recorded. Electrochemical impedance spectroscopy was performed before and after polarization to obtain the corresponding interfacial resistances (R_0 and R_s), and tLi^+ was calculated accordingly. The Li^+ transference number was calculated with the following formula:

$$t_{Li^+} = \frac{I_s(\Delta V - I_0 R_0)}{I_0(\Delta V - I_s R_s)}$$

where I_0 and R_0 are the initial current and initial resistance, respectively; while I_s and R_s are the steady-state current and steady-state resistance, respectively, and ∆V is the fixed potential value (10 mV).

CV curves were tested on the BioLogic VMP3 electrochemical workstation over a range of 1.0 to 3.0 V. The cycle and rate performance of batteries were

tested by LAND CT2001A battery test instruments. For each battery, only one rate was tested.

9. Materials characterizations:

The samples were tested by FT-IR spectroscopy using a Thermo Nicolet Nexus 470 spectrometer. Variable temperature in-situ FT-IR was tested using an EQUINOX55 spectrometer from Bruker, Germany. ^{1}H NMR spectra was tested on a Bruker 600 M spectrometer. Raman tests were conducted on the Thermo Fisher Scientific DXR.

10. Simulation details and methodology:

Quantum chemistry calculations were first performed to optimize molecular geometries of MPPE and PVDF-HFP using the Gaussian 16 package at B3LYP/6-311+G(d) level of theory. The atomic partial charges on these molecules were computed by fitting to the molecular electrostatic potential at atomic centers with the Møller-Plesset second-order perturbation method and the correlation-consistent polarized valence cc-pVTZ(-f) basis set.

Binding energies of the Li^{+}-(MPPE or PVDF-HFP) complexes were calculated after geometry optimizations, where the full complexes were optimized with and without Li^{+}, representing their separation at infinite distance.3, 4 The binding energy was calculated as:

$$E = E_{Li+-(polymer)} - (E_{Li+} + E_{(polymer)})$$

Supporting Figures

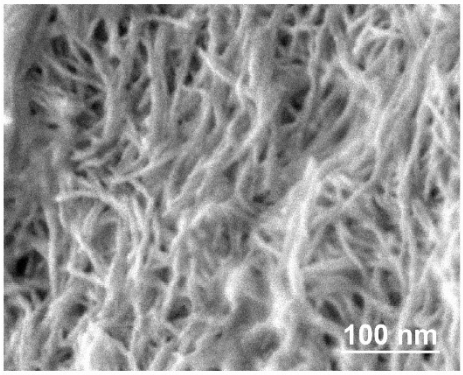

Fig. S1 | SEM images of MPPE surface.

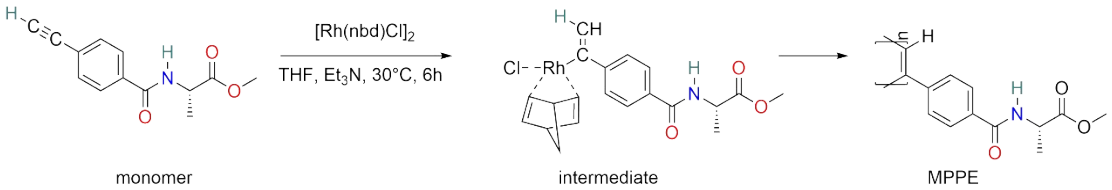

Fig. S2 | Polymerization process of MPPE.

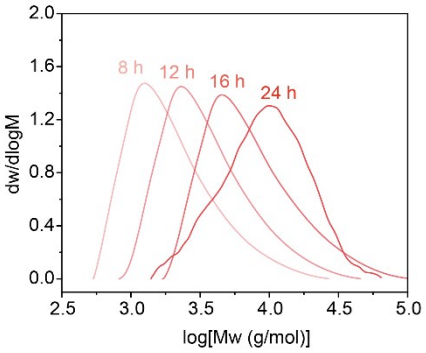

Fig. S3 | Molecular weight distribution of polymer MPPE measured by gel permeation chromatography.

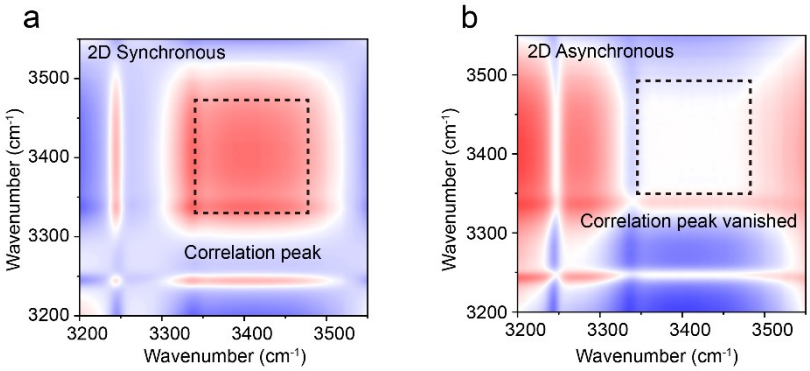

Fig. S4 | Two-dimensional synchronous and asynchronous spectra of MPPE electrolyte temperature-dependent infrared spectroscopy.

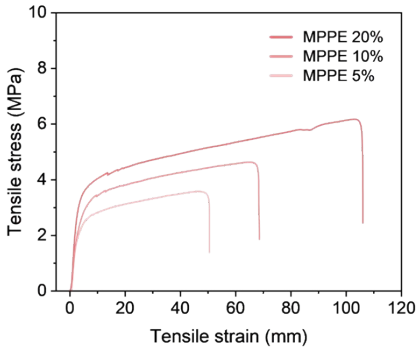

Fig. S5 | Stress-Strain curves of MPPE electrolyte membranes with different composition ratios.

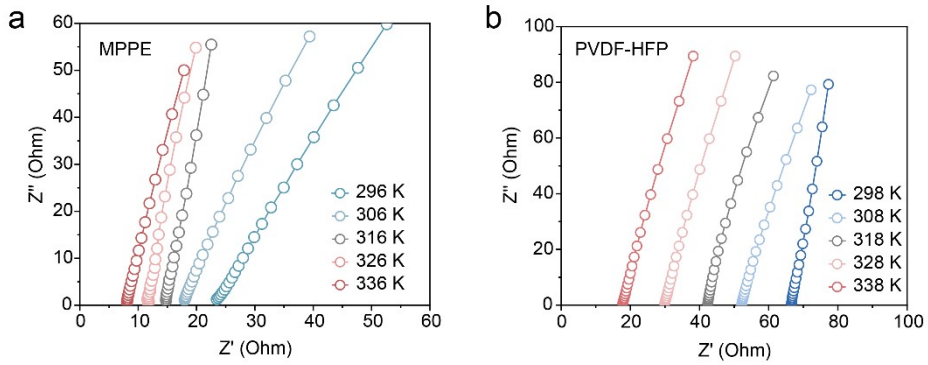

Fig. S6 | EIS impedance of symmetrical stainless steel batteries using MPPE and PVDF-HFP electrolytes at different temperatures.

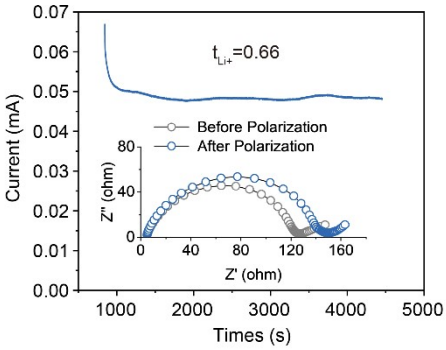

Fig. S7 | Lithium ion transfer number in PVDF-HFP electrolyte.

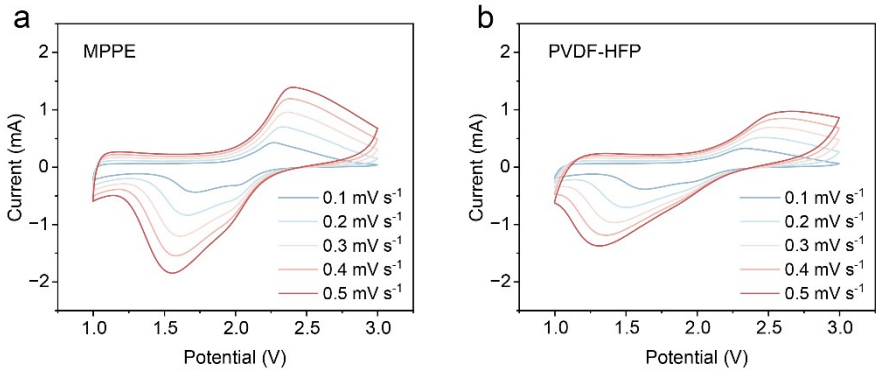

Fig. S8 | CV curves of full batteries based on MPPE and PVDF-HFP electrolytes.

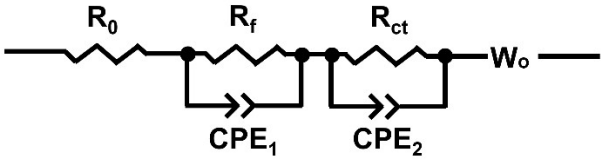

Fig. S9 | The corresponding equivalent circuit of EIS test. R_0 corresponds to bulk electrolyte resistance; $R_f||CPE_1$ and $R_{ct}||CPE_2$ represent interphase (SEI) and charge-transfer processes, respectively; W_0 accounts for diffusion at low frequency. CPEs are used instead of ideal capacitors to capture depressed semicircles arising from interfacial heterogeneity/roughness.

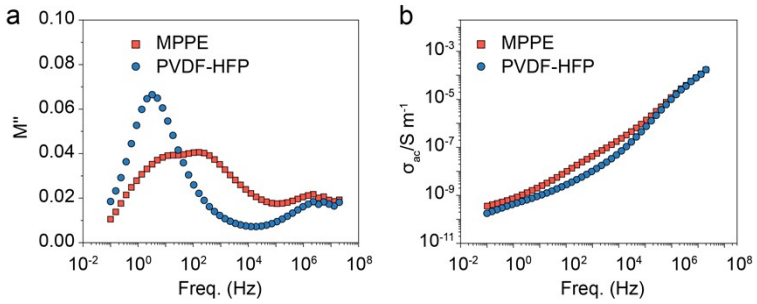

Fig. S10 | The relationship between dielectric modulus spectrum and AC conductivity of MPPE and PVDF-HFP with frequency.

Table S1 | Performance comparison of representative solid-state electrolytes for all-solid-state Li–S batteries

Electrolyte	Capacity ($mAh\ g^{-1}$)	Current density (C)	Cap. (%)	Cycles (n)	S loading ($mg\ cm^{-2}$)	Minimum operating temperature (°C)	Ref
This work	958	0.5	91	500	1	0	--
This work	773	1	91	400	1	0	--
LPE@Ni-DMF	811	1	60	1000	1	25	[5]
LPE@Ni-DMF	961	0.2	81.9	300	0.8	25	[5]
PACOF-8	750	1	65.8	1000	0.8	25	[6]
PEO-PEN	800	0.1	68.3	75	0.6	25	[7]
Solid SPAN	897	0.2	68.3	100	0.4	25	[8]
LPC@2%UCPBA	912	0.5	97.6	180	0.6	25	[9]
3D MPPL	418	0.5	77.3	400	0.68	25	[10]
PEO@P_2S_5	870	0.3	92	250	0.8	25	[11]
PTMG-HDI-BHDS	647	0.3	91	700	2	30	[12]
LPSx-5	950	0.5	60	500	1	25	[13]
PVDF&PU/LLZTO	600	0.5	77.5	230	1	0	[14]
S-EVA	1345	0.5	70	200	1.2	25	[15]
PSN@MXene	900	2	55	800	1	25	[16]
NH-$FSe_{0.03}S_{0.97}$PAN	971	1	79.6	1200	2	25	[17]
S-C-LPB	1004	0.5	77.5	800	2.57	60	[18]
S-C-MIEC20	930	2	97.6	1000	2	25	[19]
$Li_{10.1}Si_{1.5}P_{1.5}S_{11.6}I_{0.4}$	760	1	67	500	1	25	[20]
LPSC	1.96 $mAh\ cm^{-2}$	0.2	92.2	400	1.26	25	[21]
$LPSCl_{1.5}$	990	0.1	--	50	1.7	25	[22]
LPSCl	0.67 $mAh\ cm^{-2}$	0.67 $mA\ cm^{-2}$	93.2	450	2	25	[23]
S@C-0.3wt%	1300	0.05	34.6	100	--	60	[24]
TeCo-S/C	1030	0.5	84	500	2.5	25	[25]

references

[1] W. Song, B. Li, Y. Qu, W. Jiang, M. Pei, N. Hu, S. Zhuo, C. Su, X. Jin, R. Mao, D. Liu, X. Jian and F. Hu, *Angew. Chem. Int. Ed. Engl.* **2025,** *64* (29), e202505095.

[2] Z. Song, L. Wang, W. Jiang, M. Pei, B. Li, R. Mao, S. Liu, T. Zhang, X. Jian and F. Hu, *Adv. Energy Mater.* **2023,** *14* (4), 2302688.

[3] J. Holoubek, H. Liu, Z. Wu, Y. Yin, X. Xing, G. Cai, S. Yu, H. Zhou, T. A. Pascal, Z. Chen and P. Liu, *Nat. Energy* **2021,** *6*(3), *303-313.*

[4] Z. Yu, P. E. Rudnicki, Z. Zhang, Z. Huang, H. Celik, S. T. Oyakhire, Y. Chen, X. Kong, S. C. Kim, X. Xiao, H. Wang, Y. Zheng, G. A. Kamat, M. S. Kim, S. F. Bent, J. Qin, Y. Cui and Z. Bao, *Nat. Energy* **2022,** *7* (1), 94-106.

[5] Y. Zhu, Z. Lao, M. Zhang, T. Hou, X. Xiao, Z. Piao, G. Lu, Z. Han, R. Gao, L. Nie, X. Wu, Y. Song, C. Ji, J. Wang and G. Zhou, *Nat. Commun.* **2024,** *15* (1), 3914.

[6] X. Wu, W. Zhang, H. Qu, C. Guan, C. Li, G. Lu, C. Chang, Z. Lao, Y. Zhu, L. Nie and G. Zhou, *Energy Environ. Sci.* **2025**, *18*(4), 1835-1846.

[7] J. Sheng, Q. Zhang, C. Sun, J. Wang, X. Zhong, B. Chen, C. Li, R. Gao, Z. Han and G. Zhou, *Adv. Funct. Mater.* **2022,** *32* (40), 2203272.

[8] C. Li, Q. Zhang, J. Sheng, B. Chen, R. Gao, Z. Piao, X. Zhong, Z. Han, Y. Zhu, J. Wang, G. Zhou and H.-M. Cheng, *Energy Environ. Sci.* **2022,** *15* (10), 4289-4300.

[9] Y. Zhu, Q. Zhang, Y. Zheng, G. Li, R. Gao, Z. Piao, D. Luo, R. H. Gao, M. Zhang, X. Xiao, C. Li, Z. Lao, J. Wang, Z. Chen and G. Zhou, *PNAS,* **2023,** *120* (15), e2300197120.

[10] J. Li, F. Xie, W. Pang, Q. Liang, X. Yang and L. Zhang, *Sci. Adv.* **2024,** *10*(11), eadl3925.

[11] Z. Hu, C. Geng, J. Shi, Q. Li, H. Yang, M. Jiang, L. Wang, Q.-H. Yang and W. Lv, *J. Am. Chem. Soc.* **2024,** *146* (49), 34023-34032.

[12] F. Pei, L. Wu, Y. Zhang, Y. Liao, Q. Kang, Y. Han, H. Zhang, Y. Shen, H. Xu, Z. Li and Y. Huang, *Nat. Commun.* **2024,** *15* (1), 351.

[13] Y. Song, H. Qu, Z. Lao, X. Xiao, G. Lu, Y. Song, L. Nie, J. Wang, J. Yang, Y. Zhu and G. Zhou, *Adv. Mater.* **2025,** *37* (18), 2419271.

[14] L. Nie, J. Zhu, X. Wu, M. Zhang, X. Xiao, R. Gao, X. Wu, Y. Zhu, S. Chen, Z. Han, Y. Yu, S. Wang, S. Ling and G. Zhou, *Adv. Mater.* **2024,** *36* (29), 2400115.

[15] X. Zhu, W. Jiang, L. Wang and J. Lu, *Adv. Energy Mater.* **2024,** *14* (17), 2304244.

[16] Z. H. Luo, M. Zheng, M. X. Zhou, X. T. Sheng, X. L. Chen, J. J. Shao, T. S. Wang and G. Zhou, *Adv. Mater.* **2025,** *37* (9), 2417321.

[17] Q. Wu, Y. Wu, H. Yan, W. Zhong, M. Qin, H. Zhu, S. Cheng and J. Xie, *Energy Environ. Sci.* **2025**, *18*(10), 4905-4915.

[18] D. Wang, L. J. Jhang, R. Kou, M. Liao, S. Zheng, H. Jiang, P. Shi, G. X. Li, K. Meng and D. Wang, *Nat. Commun.* **2023,** *14* (1), 1895.

[19] D. Wang, B. Gwalani, D. Wierzbicki, V. Singh, L.-J. Jhang, T. Rojas, R. Kou, M. Liao, L. Ye, H. Jiang, S. Shan, A. Silver, A. T. Ngo, Y. Du, X. Li and D. Wang, *Nat. Mater.* **2025,** *24* (2), 243-251.

[20] J. Yang, R. Zhang, R. Zimmermanns, M. Schaller, S. Indris, J. Choi, S. Fleischmann, T. Brezesinski and F. Strauss, *Adv. Mater.* **2026,** *38* (15), e13204.

[21] K. Shen, W. Shi, H. Song, C. Zheng, Y. Yan, X. Hong, X. Liu, Y. An, Y. Li, F. Ye, M. He, G. Ye, C. Ma, L. Zheng, P. Gao and Q. Pang, *Adv. Mater.* **2025,** *37* (11), e2417171.

[22] Z. Yu, B. Singh, Y. Yu and L. F. Nazar, *Nat. Mater.* **2025,** *24* (7), 1082-1090.
[23] J. Lee, S. Zhou, V. C. Ferrari, C. Zhao, A. Sun, S. Nicholas, Y. Liu, C. Sun, D. Wierzbicki, D. Y. Parkinson, J. Bai, W. Xu, Y. Du, K. Amine, and G.-L. Xu, *Science,* **2025,** *388*(6748): 724-729.
[24] Y. Li, C. Wang, Y. Zhu, D. Xie, X. Chen and Y. Mei, *J. Energy Storage,* **2026,** *141*, 119248.
[25] H. Zhong, H. Lin, W. Huang, M. Su, Y. Wu, R. Ma, Y. Luo, P. Yu, S. Pan, Y. Deng, Z. Gong and Y. Yang, *ACS Energy Lett.* **2025,** *10* (9), 4082-4090.